Fizika Nizkikh Temperatur, 2002, v. 28, No. 7, p. 724–732

Light scattering on phonons in quasi-one-dimensional antiferromagnet $CsFeCl_3 \cdot 2H_2O$ induced by magnetic ordering

V. S. Kurnosov[1], Yu. G. Pashkevich[2], A. V. Peschanskii[1], V. I. Fomin[1], and A. V. Yeremenko[1]

[1]*B.Verkin Institute for Low Temperature Physics and Engineering National Academy of Sciences of the Ukraine, 47 Lenin Ave., Kharkov 61103, Ukraine*

[2]*A.Galkin Donetsk Physical and Technical Institute of the National Academy of Sciences of the Ukraine, 72 R.Luxemburg Str., Donetsk 83114, Ukraine*

E-mail:Kurnosov@ilt.kharkov.ua

Received February 1, 2002

The appearance of new phonon lines in the Raman spectrum of the quasi-one-dimensional antiferromagnet $CsFeCl_3 \cdot 2H_2O$ as a consequence of magnetic ordering with a change of the unit cell volume was detected experimentally. An analysis of the possible mechanisms that might lead to the observed spectral features is done. A new mechanism of inducing Raman scattering on phonons from the boundary of the paramagnetic Brillouin zone is hypothesized.

PACS: **71.45.-d, 78.30.–j**

Introduction

The compound $CsFeCl_3 \cdot 2H_2O$ under consideration is a representative of a family of quasi-one-dimensional chained orthorhombic magnets with a general chemical formula $AMX_3 \cdot 2H_2O$, where A = Cs, Rb, M = Mn, Fe, Co and X = Cl, Br. All these crystals have D_{2h}^8 (*Pcca*) symmetry in the paramagnetic phase [1–3]. The magnetically ordered phases of crystals of this series are described by different magnetic space groups. The magnetic cell is commonly doubled along the crystallographic direction *b* compared to the paramagnetic one [1,4,5]. The $CsFeCl_3 \cdot 2H_2O$ and $RbFeCl_3 \cdot 2H_2O$ crystals are attracting interest because they are an Ising type of antiferromagnet, unlike the Heisenberg type observed in $CsMnCl_3 \cdot 2H_2O$ [1]. Moreover, the Dzyaloshinski–Moriya interaction produces a considerable canting of the spins in the antiferromagnetic phase (AF) of $CsFeCl_3 \cdot 2H_2O$ and $RbFeCl_3 \cdot 2H_2O$, resulting in an uncompensated magnetic moment within each of the paramagnetic ion chains. The total momentum of the crystals remains zero because of the alternating direction of the moments in neighboring chains. The magnetic moments of the chains are oriented in parallel with the crystallographic axis *c* of the crystals, and therefore, application of an external field along this direction can induce a first-order phase transition (PT) to a weak ferromagnetic (WF) phase [1]. A specific feature of this PT is the fact that the flip–flop of all the spins of the paramagnetic ions in each separate chain occurs through the motion of a magnetic soliton along the chain. Besides, this PT occurs with the passage of the crystal through a number of metastable intermediate phases which are characterized by different ratios between the numbers of chains with the ferromagnetic moment oriented along and opposite to the applied field [1,6,7].

Despite the great number of experimental studies of $CsFeCl_3 \cdot 2H_2O$ motivated by its interesting magnetic properties, very few of them were carried out using optical methods. Among the experiments known to the authors, only the experiments on excitonic absorption of light in the visible range have been performed in high magnetic fields (up to those of the metamagnetic transition) [8–10]. Since not all the crystals of the above family undergo

structure phase transitions, while their structures are almost similar, Raman and IR spectroscopy measurements of their vibrational spectra have not aroused particular interest. Moreover, the vibrational spectra of one of the earliest representatives of the family, namely, $CsMnCl_3 \cdot 2H_2O$, have been previously studied comprehensively, including by the authors of the present paper [11–13]. The experiments reported here were motivated by the authors' interest in the specific features of the Raman scattering in the magnetically ordered phase of $CsFeCl_3 \cdot 2H_2O$ (referred to below as CFC). Foremost among these is light scattering by magnons, quite possibly by solitons. Besides, the fact that an Fe^{2+} ion has low-energy electron levels generated due to the splitting of its ground term $^5T_2$ in a low-symmetry crystal field suggests the occurrence of electronic transitions active in the Raman scattering in the low-frequency spectrum.

The experiment performed demonstrated that at the temperatures below the Néel point (T_N = 12.75 K [7]) the Raman spectrum of the crystalwas much richer than that of $CsMnCl_3 \cdot 2H_2O$ (CMC). But at temperatures much above the magnetic ordering points in CMC and CFC these spectra are quite similar. The low-temperature Raman spectrum of CFC displays additional lines as against the spectrum of CMC, the lines being differently sensitive to variations in temperature of the crystal and external magnetic field. Some of the lines have intensity comparable to the intensity of the strongest lines of the original phonon spectrum of CFC, which disappear on transition of the crystal to a paramagnetic (PM) (in temperature) or a WF (in field) phase. The present paper concerns mainly the nature of these lines and the physical reasons for their occurrence in the Raman spectrum.

Experimental procedure

The transparent pale brown single crystals of CFC were grown from an aqueous solution of CsCl and $FeCl_2 \cdot 4H_2O$ by slow evaporation at T = 37° C in a nitrogen atmosphere to prevent Fe^{2+} oxidation [1,9]. The single crystals keep well in oxygen-free gaseous atmospheres. The adjustment of the crystallographic directions was made according to a well-defined habit, similar to that of CMC [4]. Samples in the form of rectangular parallelepipeds with dimensions of 6×5×2 mm were cut from the single crystals and polished up to optical quality of the surface. The sample faces were oriented in parallel with the principal crystallographic planes of the crystal. The Cartesian coordinate system used was related to the crystallographic directions as $x \parallel a$, $y \parallel b$, $z \parallel c$.

The measurements were carried out in two types of optical cryostats: (i) one type permitted the experiments to be done in a wide temperature range of 4.2 to 300 K, and (ii) the other one had a two-section Helmholtz superconducting solenoid for performing the measurements in an exchange gas of liquid helium at ~4.2 K at magnetic field strengths up to 30 kOe. The Raman scattering was excited by He–Ne and Ar^+ laser radiation (wavelength 6328 Å, power 40 mW, and wavelength 4880 Å, power 120 mW). The 90° scattered light was analyzed with a computerized Raman spectrometer based on a Jobin Yvon U-1000 double monochromator which was equipped with a cooled photomultiplier and a photon counting system. The signal–noise ratio was improved by the spectrum acquisition method with a multiple scanning of the frequency range studied.

The use of the two light sources was dictated by several reasons. In experiments with Raman scattering the illumination of a sample by a focused laser beam produces a higher overheating in the laser beam zone, relative to the sample surface, the higher the absorption at the laser wavelength. Since the crystal optical transmission at the He–Ne laser wavelength of 6328 Å is higher, that source appeared to be more attractive for the experiments. Despite the fact that the argon laser produces a much more intense overheating of the sample, it was used for the measurements in magnetic field because the solenoid drastically confines the angular aperture of the scattered light and hence, decreases significantly the intensity of the signal detected. In that case the benefit that permitted us to compensate the aperture loss consisted of two components: first, a high radiation power, and, second, the Rayleigh $1/\lambda^4$ law for the Raman scattering intensity.

Experimental results

The Raman scattering spectrum of the CFC crystal studied at temperatures below T_N revealed two intense (182 and 501 cm^{-1}) and four weak (125, 130, 140, and 607 cm^{-1}) lines, with polarization corresponding to the diagonal components of the scattering tensor. The distinguishing feature of these lines is the fact that their intensities decrease rather fast with increasing temperature in the immediate vicinity of T_N and that they almost disappear at higher temperatures (Fig. 1). But the «additional» lines undergo no noticeable variations in frequency and width. It should be

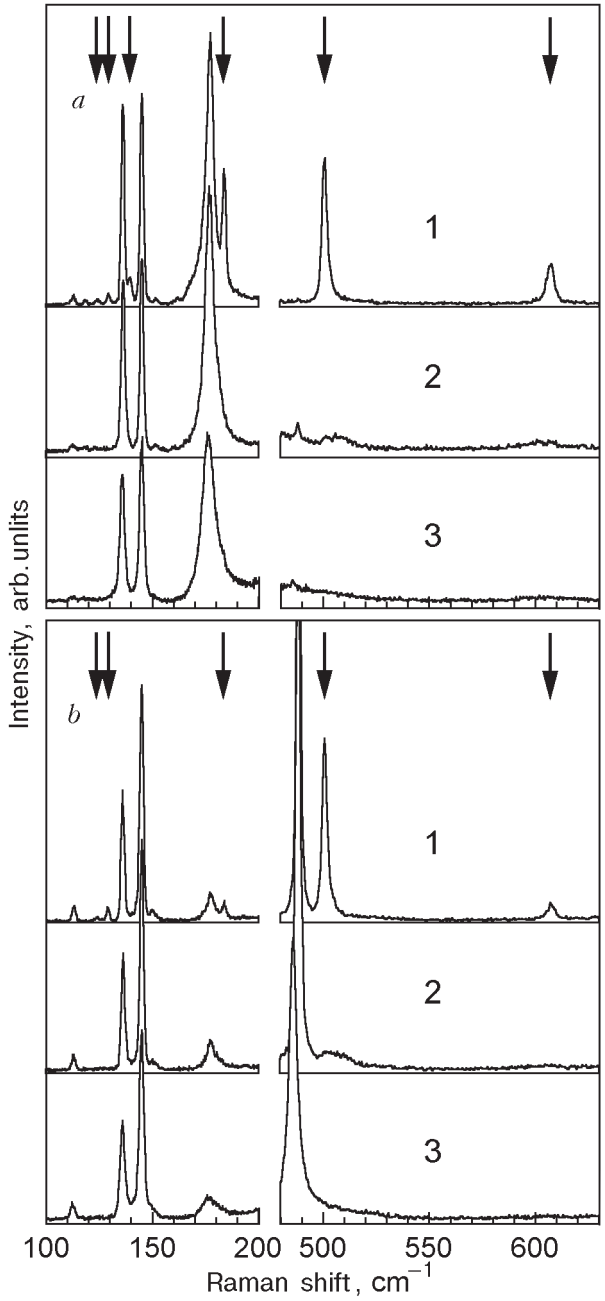

Fig. 1. Parts of the Raman spectrum of $CsFeCl_3 \cdot 2H_2O$ corresponding to scattering tensor components *yy* (*a*) and *zz* (*b*) at temperatures, K: 5 (*1*), 25 (*2*), and 80 (*3*). The «additional» lines (see the text) are marked by arrows. The spectral resolution is 2 cm^{-1}.

noted that lines «additional» to the original phonon spectrum can be also observed in the spectrum with off-diagonal components of the Raman tensor at temperatures below T_N . Those lines, however, are all of low intensity compared to the lines of the original phonon spectrum and do not exhibit distinctly the above-mentioned temperature dependence*.

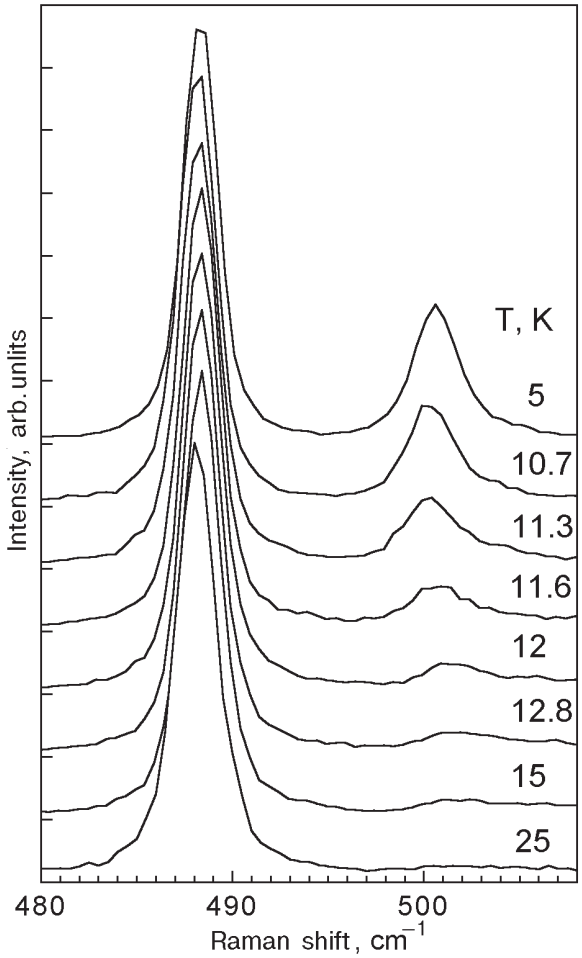

Fig. 2. The temperature evolution of part of the Raman spectrum with scattering tensor component *zz* for $CsFeCl_3 \cdot 2H_2O$.

The temperature evolution of the most intense lines, of frequencies 182 and 501 cm^{-1}, is shown in Figs. 2 and 3. The 488 and 177 cm^{-1} lines in the spectra correspond to the phonons of the original vibrational spectrum of the crystal and show no anomalous behavior in the temperature range given in the figures. The temperature dependence of the 182 cm^{-1} line area correlates well with the Néel temperature (Fig. 4). The temperature in these experiments was determined by the ratio of intensities of Stokes and anti-Stokes scattering at the lowest-frequency phonon (~30 cm^{-1}) in the crystal. This ratio satisfies the relation:

$$I_s / I_a = \exp \frac{\hbar\omega}{kT},$$

* The nature of these exitations will be considered in a separate paper.

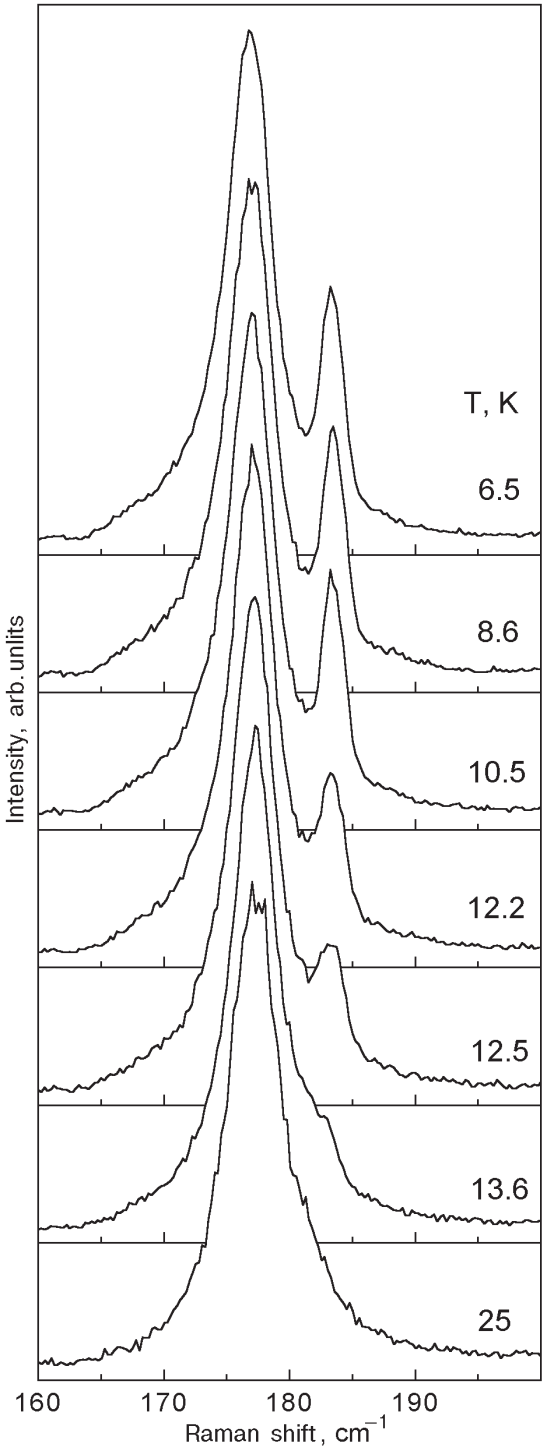

Fig. 3. The temperature evolution of part of the Raman spectrum with scattering tensor component *yy* for $CsFeCl_3 \cdot 2H_2O$.

where I_s and I_a are the Stokes and anti-Stokes components of the scattering on a phonon of energy $\hbar\omega$; T is the temperature, and k is the Boltzmann constant.

The measurements with the magnetic field directed along the crystal axis *c* show that the 182 cm^{-1} line intensity decreases rapidly as the magnetic field strength approaches a critical value, at which one can observe a PT to a new magnetic phase [1,6] (Fig. 5). The relation between intensity of the line and cyclic variations in intensity of the applied magnetic field is illustrated in Fig. 6.

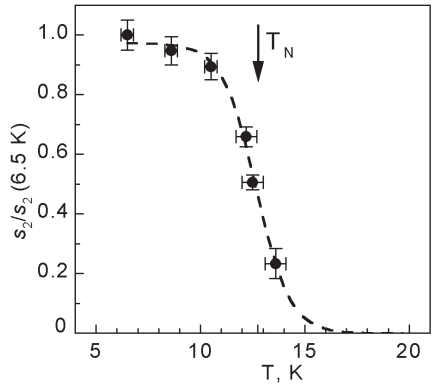

Fig. 4. The temperature dependence of relative area of the 182 cm^{-1} line in $CsFeCl_3 \cdot 2H_2O$. To make the figure more pictorial, the dashed line is plotted by eye.

Discussion of the experimental results

To account for the experimental results, some specific features of the crystallographic and magnetic structures of CFC should be considered.

Magnetism of CFC

In the magnetically ordered phase of CFC an octasublattice structure (Fig. 7,*a*), the symmetry of which is described by magnetic space group $P_{2b}cca'$, is realized [1]. The available literature data [1,6,7] suggest that the magnetic structure of CFC is formed under the action of dominant antiferromagnetic superexchange interaction along the chains consisting of *cis*-octahedra of $FeCl_4O_2$ bound together by common apical ions Cl^-. The chains in the structure of the crystal are oriented along the *a* direction. The orbital and spin degeneracies of the ground state $^5T_2$ of the Fe^{2+} ion are completely lifted theby crystal-field effect of low symmetry C_2 and the spin–orbit interaction.

The three-dimensional ordering of the magnetic moments (antiferromagnetic in all directions to nearest neighbors) is brought about by the interchain superexchange, which is at least two orders of magnitude weaker than the intrachain one [1]. As a result, the magnetic cell appears to be doubled along the crystallographic direction *b* as compared to the paramagnetic one. Also noteworthy is the high value of the Dzyaloshinski–Moriya interaction, which causes the spins to be canted from the *a* direction by an angle of 15° in the *ac* plane [1]. This

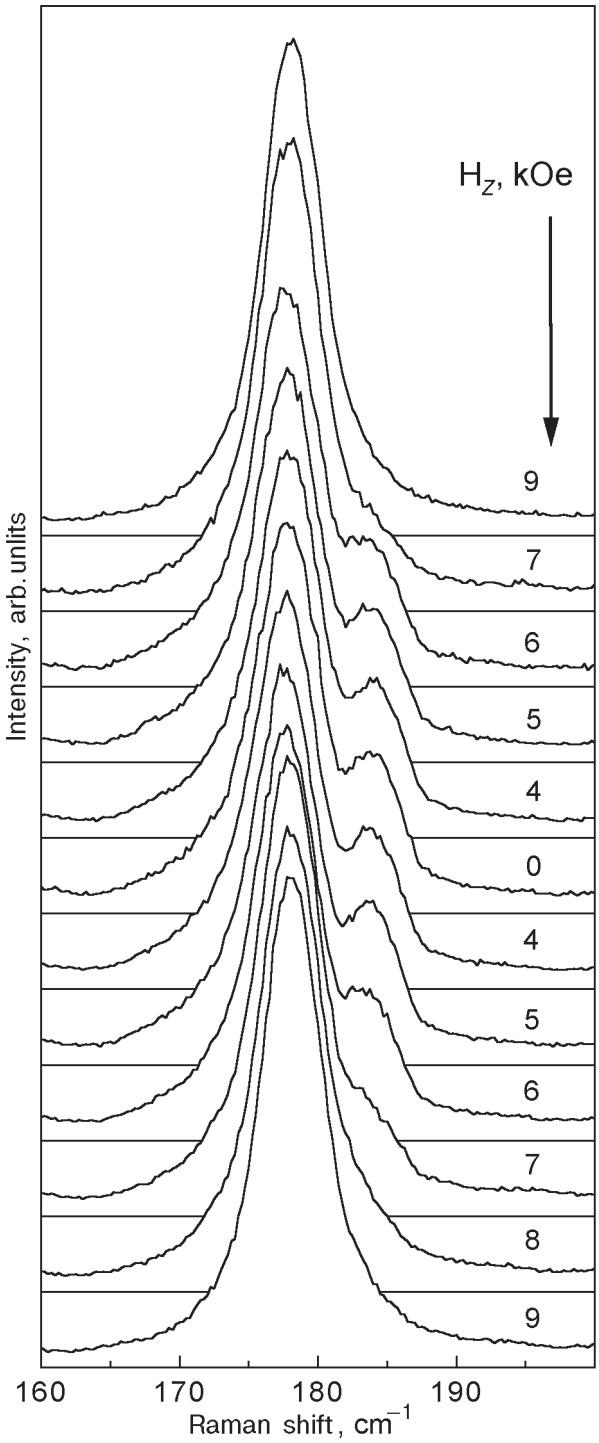

Fig. 5. The part of the Raman spectrum with scattering tensor component *yy* as a function of the external magnetic field H_Z in $CsFeCl_3 \cdot 2H_2O$. The sample temperature is ~11 K. The spectral resolution is ~ 3 cm^{-1}.

canting results in a ferromagnetic moment of each individual chain in the crystal which is directed collinearly with the *c* axis. The moments of all chains in the crystal compensate each other due to antiferromagnetic ordering of nearest spins of

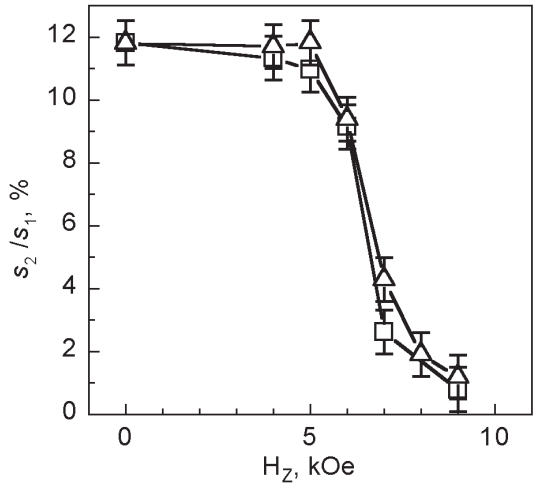

Fig. 6. The plot of the area ratio of the 182 and 177 cm^{-1} lines shown in Fig. 5 versus magnetic field. The branches with increasing and decreasing field are denoted by squares and triangles, respectively.

neighboring chains, so that the total magnetic moment of the crystal is zero.

On application of an external magnetic field of intensity ~9.5 kOe along the *c* axis, the crystal undergoes a PT at temperatures below T_N [1,6,7]. As a result, the ferromagnetic moments of all chains become oriented along the field direction (Fig. 7,*b*). It should be emphasized that in the new phase the neighboring chains along the *b* direction are found to be translationally equivalent once again, and the magnetic cell volume reverts to the volume of the paramagnetic cell. The WF phase symmetry is described by space group

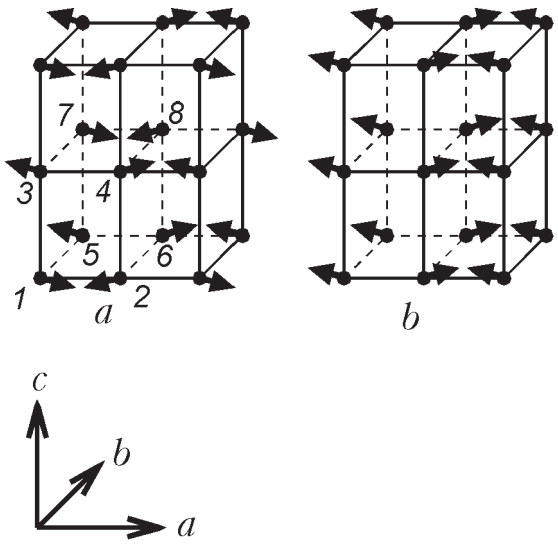

Fig. 7. The magnetic structure of $CsFeCl_3 \cdot 2H_2O$ in antiferromagnetic (*a*) and weak ferromagnetic (*b*) phases.

$Pc'c'a$. During «magnetization» the crystal actually undergoes a number of transitions through the multitude of intermediate phases with a different specific number of chains with «inverted» (compared to the normal AF phase) ferromagnetic moments [7]. The moderate intensity of the magnetic field at which this PT occurs is accounted for by the small values of the interchain exchange interaction integrals along the c and b directions. As for the magnetic structure inside the chain, it remains almost unchanged in such weak fields, because it is stabilized by the high single-ion anisotropy and intrachain exchange.

In terms of the Heisenberg approximation, the magnetic parameters can be described by the following values of exchange integral J_a/k = 6.0 ± 0.5 K and single-ion anisotropy constant D/k = −40 ± 20 K with total spin S = 2 [6]. With these relations of the model parameters, the magnet at low temperatures may be approximated by the Ising model with effective spin $S_{\text{eff}} = 1/2$ and effective exchange integral J_{eff}/k = 42 ± 5 K [6].

Analysis of the Raman spectrum

The specific features of the Raman spectrum of CFC, manifesting themselves as additional (to the original phonon spectrum) lines in the magnetic phase, may be brought about by different mechanisms.

First, it should be noted that according to all the available published data, CFC, along with other representatives of this family of crystals, undergoes no structural PT. The fact is evidenced by the authors' observations. No peculiarities in the temperature behavior of the Raman spectrum which are accounted for by a structural phase transition followed by a multiplication of the unit cell volume were found. The soft mode usual at such PTs is not observed in the low-temperature phase. In the following, the authors will proceed from the fact that there are no phase transitions in CFC.

As mentioned in the Introduction, aside from the phonon excitations, the low-frequency Raman spectrum of CFC can contain lines caused by a scattering owing to the transition between crystal-field-split levels of the ground state term of the Fe^{2+} ion, and scattering by magnons. Turning back to the main point of the present paper, namely, to the treatment of the anomalous behavior of the additional scattering lines of frequencies 125, 130, 140, 182, and 501 cm^{-1} (Fig. 1), we should consider some possible mechanisms. To do this, we should first estimate the energy range within which the magnon scattering may be observed.

In terms of the Heisenberg approach for a one-dimensional chain of spins, the magnon energy dispersion within the one-dimensional Brillouin zone (BZ) can be given as follows:

$$E(\varphi) = 2JS\left[\left(1 + \frac{|D|}{2JS}\right)^2 - \cos^2\varphi\right]^{1/2},$$

where φ is the spatial phase of a spin wave in the a direction. Using this equation, one can obtain the following estimates of magnon energies at the center and at the boundary of the one-dimensional BZ: $E(0)$ = 42 cm^{-1}, $E(\pi/2)$ = 46 cm^{-1}. In terms of the Ising model, the magnon energy at the BZ boundary, $E(\pi/2) = 4J_{\text{eff}}S_{\text{eff}}$, is estimated as being equal to 58 cm^{-1}. Besides the energy of the optical magnon, the transition from the lowest component of the electron pseudo-doublet, with a total momentum projection of ±1, to the first excited singlet level, with a projection of 0, is estimated to be 80 cm^{-1} [10]. All these simple estimates are rather rough, but they make it possible to place an upper limit on the energy range in which the magnon spectrum may manifest itself: to 100 cm^{-1}. Therefore, it is hardly probable that additional lines disappearing from the scattering spectrum at temperatures above T_N are accounted for by the magnon scattering. The two-magnon scattering, which may fall just within the frequency range studied, rarely, if ever, is of high intensity in the diagonal components of the scattering tensor. Besides, it is primary conditioned on the strong exchange along the chains which is essentially un affected by the magnetic field applied in our experiments (see above).

The electron transitions also evident in the Raman spectrum of CFC exhibit a somewhat different (compared to the lines considered) evolution with increasing temperature. The electron lines in the Raman spectrum also show the decrease in area with increasing temperature, but this occurs at much higher temperatures (above 70 K in CFC) and is followed by a drastic broadening of the lines. The latter fact does not allow the suggestion that the lines are unobservable because the integral intensity vanishes. Thus the additional lines under consideration cannot be ascribed to scattering by electron transitions either.

Another feature of the magnetic structure of CFC mentioned above is the double volume of the unit cell compared to the paramagnetic one. This doubling, determined by neutron scattering [1], is solely of a magnetic nature without any structural distortion. A double-unit-cell crystal is thought to exhibit a larger number of phonon modes in the

Raman spectrum, the additional lines appearing at the magnetic BZ center from the paramagnetic BZ boundary. Despite this formal concept, there are very few experimental works on Raman scattering by phonons generated from the paramagnetic BZ boundary under magnetic ordering with a unit cell multiplication.

In the case of CFC two facts have permitted the authors to suggest that the additional lines under consideration are indeed related to scattering by phonons generated from the paramagnetic BZ boundary. These are, first, the temperature dependence, showing a fast decrease in intensity of the lines in the vicinity of T_N and their absence at higher temperatures, and, second, the field dependence of the intensity of these lines. The latter for the most intense line of frequency 177 cm^{-1} demonstrates a behavior similar to the temperature dependence. When the unit cell volume returns to the paramagnetic volume, either as a result of the temperature increasing or as a result of a PT in an external magnetic field, the additional lines disappear from the Raman spectrum.

A formal increase in the number of Raman-active phonons resulting from the doubling of the unit cell volume in the magnetically ordered phase cannot explain the physical mechanisms which are responsible for the additional phonon lines in the Raman spectrum. There must be a reason causing nonequivalence of the polarizabilities associated with vibrations of the same ions from neighboring cells along the doubling direction. Otherwise, because the vibrations of identical ions in the modes from the BZ boundary are opposite in phase, the intensity of Raman scattering by them should be zero due to the complete interference damping. As a matter of fact, this is an example of the wave-vector **k** selection rule for light scattering or absorption (the **k** = 0 rule).

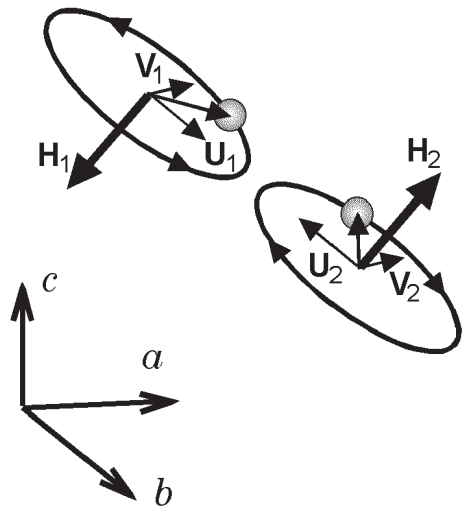

Fig. 8. The trajectory ellipticity of identical ions from neighboring-in-direction *b* cells in local magnetic fields $\mathbf{H}_1$ and $\mathbf{H}_2$. $\mathbf{U}_1$ and $\mathbf{U}_2$ are antiphase displacement components for the mode from the paramagnetic BZ boundary, $\mathbf{V}_1$ and $\mathbf{V}_2$ are in-phase displacement components induced by the Lorentz force.

Table

Irreducible spin combinations (ISC) in CFC at points $\mathbf{k}_{19} = (0,0,0)$ and $\mathbf{k}_{21} = (0,\pi/b,0)$ of the paramagnetic BZ and at the center of antiferromagnetic BZ reduced along **b** (the symbols are taken from [14] and spin numbers from Fig. 7).

ISC	PM phase	AF phase
$\mathbf{F}(0)$	$\mathbf{S}_1(0)+\mathbf{S}_2(0)+\mathbf{S}_3(0)+\mathbf{S}_4(0)$	$\mathbf{S}_1+\mathbf{S}_2+\mathbf{S}_3+\mathbf{S}_4+\mathbf{S}_5+\mathbf{S}_6+\mathbf{S}_7+\mathbf{S}_8$
$\mathbf{L}_1(0)$	$\mathbf{S}_1(0)+\mathbf{S}_2(0)-\mathbf{S}_3(0)-\mathbf{S}_4(0)$	$\mathbf{S}_1+\mathbf{S}_2-\mathbf{S}_3-\mathbf{S}_4+\mathbf{S}_5+\mathbf{S}_6-\mathbf{S}_7-\mathbf{S}_8$
$\mathbf{L}_2(0)$	$\mathbf{S}_1(0)-\mathbf{S}_2(0)+\mathbf{S}_3(0)-\mathbf{S}_4(0)$	$\mathbf{S}_1-\mathbf{S}_2+\mathbf{S}_3-\mathbf{S}_4+\mathbf{S}_5-\mathbf{S}_6+\mathbf{S}_7-\mathbf{S}_8$
$\mathbf{L}_3(0)$	$\mathbf{S}_1(0)-\mathbf{S}_2(0)-\mathbf{S}_3(0)+\mathbf{S}_4(0)$	$\mathbf{S}_1-\mathbf{S}_2-\mathbf{S}_3+\mathbf{S}_4+\mathbf{S}_5-\mathbf{S}_6-\mathbf{S}_7+\mathbf{S}_8$
$\mathbf{F}(\mathbf{k}_{21})$	$\mathbf{S}_1(\mathbf{k}_{21})+\mathbf{S}_2(\mathbf{k}_{21})+\mathbf{S}_3(\mathbf{k}_{21})+\mathbf{S}_4(\mathbf{k}_{21})$	$\mathbf{S}_1+\mathbf{S}_2+\mathbf{S}_3+\mathbf{S}_4-\mathbf{S}_5-\mathbf{S}_6-\mathbf{S}_7-\mathbf{S}_8$
$\mathbf{L}_1(\mathbf{k}_{21})$	$\mathbf{S}_1(\mathbf{k}_{21})+\mathbf{S}_2(\mathbf{k}_{21})-\mathbf{S}_3(\mathbf{k}_{21})-\mathbf{S}_4(\mathbf{k}_{21})$	$\mathbf{S}_1+\mathbf{S}_2-\mathbf{S}_3-\mathbf{S}_4-\mathbf{S}_5-\mathbf{S}_6+\mathbf{S}_7+\mathbf{S}_8$
$\mathbf{L}_2(\mathbf{k}_{21})$	$\mathbf{S}_1(\mathbf{k}_{21})-\mathbf{S}_2(\mathbf{k}_{21})+\mathbf{S}_3(\mathbf{k}_{21})-\mathbf{S}_4(\mathbf{k}_{21})$	$\mathbf{S}_1-\mathbf{S}_2+\mathbf{S}_3-\mathbf{S}_4-\mathbf{S}_5+\mathbf{S}_6-\mathbf{S}_7+\mathbf{S}_8$
$\mathbf{L}_3(\mathbf{k}_{21})$	$\mathbf{S}_1(\mathbf{k}_{21})-\mathbf{S}_2(\mathbf{k}_{21})-\mathbf{S}_3(\mathbf{k}_{21})+\mathbf{S}_4(\mathbf{k}_{21})$	$\mathbf{S}_1-\mathbf{S}_2-\mathbf{S}_3+\mathbf{S}_4-\mathbf{S}_5+\mathbf{S}_6+\mathbf{S}_7-\mathbf{S}_8$

Symmetry analysis of polarizability

The phase transition to a magnetically ordered phase $P_{2b}cca'$ (see Table) occurs at the point $\mathbf{k}_{21}$ of the paramagnetic BZ and is described by the order parameter $L_{3x}(\mathbf{k}_{21})$ or $L_{1z}(\mathbf{k}_{21})$ which transforms according to the irreducible representation $\tau_3(\mathbf{k}_{21})$. For the required polarizability α_{ij}^{ν} to be obtained, the dielectric permittivity tensor ε_{ij} should be expanded in normal coordinates of the vibrational modes U_ν at the paramagnetic BZ point $\mathbf{k}_{21}$ and in the magnetic vector η_μ corresponding to the order parameter. The latter describes the static perturbation of the medium due to the PT. The so-called «Faraday» (linear in magnetic vector) term in the expansion is of the following form at $\mathbf{k}_{19} = 0$:

$$\alpha_{ij}^{\nu} = \left\langle \frac{\partial^2 \varepsilon_{ij}}{\partial \eta \partial U} \eta_\mu(\mathbf{k}_{21}) U_\nu(-\mathbf{k}_{21}) \right\rangle,$$

where $\eta_\mu(\mathbf{k}_{21}) \equiv L_{3x}(\mathbf{k}_{21}) / \tau(\mathbf{k}_{21})$.

The nonzero polarizability tensors correspond only to the vibrational modes transforming according to the irreducible representations $\tau_6(\mathbf{k}_{21})$ and $\tau_7(\mathbf{k}_{21})$ and are of the forms:

$$\alpha^{\tau_6(\mathbf{k}_{21})} = \begin{pmatrix} . & d & . \\ -d & . & . \\ . & . & . \end{pmatrix}, \quad \alpha^{\tau_7(\mathbf{k}_{21})} = \begin{pmatrix} . & . & f \\ . & . & . \\ -f & . & . \end{pmatrix}.$$

As is evident from the above analysis, under magnetic ordering the paramagnetic BZ boundary may induce only those lines which in the low-temperature phase are related to phonons of symmetries B_{1g} and B_{2g}, while the observed additional lines show symmetry A_g and occur in the diagonal components of the scattering tensor. Hence, the first order of perturbation theory cannot explain the anomalies under consideration.

Another mechanism that permits one to derive the required polarization selection rules for phonon modes generated from the paramagnetic BZ boundary under magnetic ordering can be illustrated as follows.

Since there exists a nonzero local magnetic field on ligands surrounding the paramagnetic ion, then during motion in the vibrational mode there may occur a Lorentz force perpendicular to the direction of the ion displacement. Hence, the linear trajectory of the ion motion transforms to an elliptical one. In this case the directions of traversing the ellipse are opposite because the identical ions from neighboring unit cells along the direction of doubling in the magnetic cell are connected by the antitranslation operation. Thus, for the phonon mode originating from the paramagnetic BZ boundary, where the displacements, of ions with no local magnetic field are opposite in phase, the perpendicular components of the displacements, generated by the Lorentz force, appear to be in-phase. This mechanism is illustrated schematically in Fig. 8.

As the Lorentz force is of relativistic origin it is hard to suggest that it may produce a sufficient degree of ellipticity to induce intense lines of light scattering comparable with those of the original spectrum. This hypothesis, however, does have meaning if it is remembered that the mixing of different-symmetry vibrational modes corresponding to the paramagnetic BZ boundary and center occurs just in this way. If the modes are close in frequency, this channel may enhance the intensity of the additional lines at the expense of the original ones. At least, this mechanism appears to be appropriate for description of the 177 and 182 cm^{-1} modes. They have close frequencies, and the 177 cm^{-1} line of the original phonon spectrum is sufficiently wide, even at low temperatures, to overlap 182 cm^{-1} line resonantly (Fig. 3). The resonance effects are also supported by the asymmetric complex shape of the 177 cm^{-1} line at low temperatures, which becomes symmetric in the PM and WF phase in external magnetic fields (Figs. 3 and 5).

At the moment the authors propose the above mechanism as a possibility. Verification of its adequacy requires a further, more comprehensive study into the anomalies of the scattering spectrum of CFC and a development of microscopic theoretical models which would enable the above spectral features arising upon magnetic ordering to be estimated numerically.

Conclusions

The experiments with the quasi-one-dimensional chained antiferromagnet $CsFeCl_3 \cdot 2H_2O$ revealed additional, quite intense lines in the Raman spectrum at the phase transition to a magnetically ordered phase, followed by changes in the volume of the crystal magnetic cell.

It is found that in an external magnetic field the most intense additional line of 182 cm^{-1} disappears at the phase transition to a weak ferromagnetic phase.

Analysis of the symmetry of the paramagnetic, antiferromagnetic, and weak ferromagnetic structures of the crystal suggests that the new lines result from the magnetic-ordering-induced light scattering by phonons originating from the paramagnetic BZ boundary.

Analysis of the magnetic contribution to the phonon polarizability of the crystal made in the first order of perturbation theory showed no correlation with the experimental polarization selection rules for the additional lines.

A new mechanism of inducing light scattering by vibrational modes corresponding to the phonons from the paramagnetic BZ boundary is hipothesized. It is based on the mixing of different-symmetry modes from the BZ center and boundary due to the ellipticity of the ion trajectory of vibrations in their local magnetic field.

The authors are very grateful to Prof. V.V. Eremenko for his constant interest in this research and for helpful discussion.

1. J. A. J. Basten, Q. A. G. van Vlimmeren, and W. J. M. de Jonge, *Phys. Rev*. **B18**, 2179 (1978).
2. S. J. Jensen, P. Andersen, and S. R. Rasmussen, *Acta Chem. Scand*. **16**, 1890 (1962).
3. N. Thorup and H. Soling, *Acta Chem. Scand*. **23**, 2933 (1969).
4. R. D. Spence, W. J. M. de Jonge, and K. W. S. Rama Rao, *J. Chem. Phys*. **51**, 4694 (1969).
5. A. Herweijer, W. J. M. de Jonge, A. C. Botterman, A. L. M. Bongaarts, and J. A. Cowen, *Phys. Rev*. **B5**, 4618 (1972).
6. K. Kopinga, M. Steiner, and W. J. M. de Jonge, *J. Phys*. **C18**, 3511 (1985).
7. J. P. M. Smeets, E. Frikkee, W. J. M. de Jonge, and K. Kopinga, *Phys. Rev*. **B31**, 7323 (1985).
8. M. Takeda, G. Kido, I. Mogi, Y. Nakawaga, H. Okada, and N. Kojima, *J. Phys. Soc. Jpn*. **58**, 3418 (1989).
9. I. Mogi, M. Takeda, G. Kido, Y. Nakawaga, H. Okada, and N. Kojima, *J. Magn. Magn. Mater*. **104-107**, 1061 (1992).
10. H. Okada, N. Kojima, T. Ban, and I. Tsujikawa, *Phys. Rev*. **B42**, 11610 (1990).
11. D. M. Adams and D. Newton, *J. Chem. Soc*. **A22**, 3499 (1971).
12. V. P. Gnezdilov, V. V. Eremenko, V. S. Kurnosov, and V. I. Fomin, *Fiz. Nizk. Temp.* **17**, 630 (1991) [*Sov. J. Low Temp. Phys.* **17**, 331 (1991)].
13. W. Jia, E. Strauss, W. M. Yen, K. Xia, and M. Zhao, *Phys. Rev*. **B39**, 12853 (1989).
14. O. V. Kovalev. *Irreducible and Induced Representations and Co-Representations of the Fedorov's Groups,* Nauka, Moscow (1986) (in Russian).